Towards a nanostructured thermoelectric generator using ion-track lithography

E Koukharenko[1], X Li[2], I Nandhakumar[2], N Frety[3], S P Beeby[1], D Cox[4],
M J Tudor[1], B Schiedt[5], C Trautmann[5], A Bertsch[6] and N M White[1]

[1] University of Southampton, Southampton, UK
[2] School of Chemistry, Southampton, UK
[3] Institut Charles Gerhardt-Equipe PMOF Université Montpellier II, France
[4] Advanced Technology Institute, University of Surrey, UK
[5] GSI, Materialforschung, Darmstadt, Germany
[6] EPFL FSTI LMIS4 Lausanne, Switzerland

E-mail: ak@ecs.soton.ac.uk

Abstract
This paper presents the process development towards a new generation of nanostructured thermoelectric generators for power harvesting from small temperature gradients by using a combination of traditional silicon microfabrication techniques, electroplating and submicron ion-track nanolithography. Polyimide nanotemplates with pore diameters ranging from 30 nm to 120 nm were fabricated. Preliminary results from the fabrication of poly(methyl methacrylate) (PMMA)-nanostructured templates are reported. Bi_2Te_3 nanowires (80 and 120 nm diameters) were electroplated into polyimide ion-track nanotemplates. Bi_2Te_3 nanowires of a R3 m structure, with preferential orientation in (1 1 0) crystallographic plans, were electroplated. The chemical composition of Bi_2Te_3 with nearly stoichiometric composition ($Bi_{2.31}Te_3$) was obtained. Homogeneity profiles of the chemical composition were obtained. A fine-grained observed microstructure (6–10 nm) and (1 1 0) crystalline orientation were obtained, which is extremely promising for improving the thermoelectric material properties. The thermoelectric properties of the Bi_2Te_3-electroplated thin films (Seebeck coefficient α) and electrical resistivity of the Bi_2Te_3 bundle nanowires were found to be $-52\ \mu V\ K^{-1}$ and $\sim 14\ M\Omega$ cm, respectively. Polyimide (Kapton foil) and PMMA 950 photoresists were promising materials for the realization of a nanostructured thermoelectric generator on flexible and rigid substrates, respectively.

(Some figures in this article are in colour only in the electronic version)

1. Introduction

Nanostructured materials have attracted great interest in recent years because they exhibit unique physical, chemical and mechanical properties, which have extensive potential applications [1, 2]. The significantly different physical properties of these novel materials have been explained by their characteristic structural features, which are in between isolated atoms and bulk macroscopic materials [3]. In particular, the exceptional electronic, mechanical, optical, magnetic and thermoelectric (TE) properties of the nanoscale materials are due to the effect of quantum confinement, which can be attributed to the changes in the total energy and structure of the system [4]. For this reason, 1D nanostructures have a profound impact on nanoelectronics, nanodevices and alternative energy resources. Nearly every class of traditional material has a 1D-nanostructure counterpart.

The motivation of this work is to contribute to one of the great challenges in the twenty-first century: the development of alternative energy sources. In response to the needs of modern society and emerging ecological concerns, it is essential that new, low-cost and environmentally friendly energy conversion and storage systems are found. Additionally, the rapid increase in the development of remote

1

wireless devices, embedded structures and portable electronics demonstrates the need for self-sufficient local power sources. The powering of wireless devices from energy harvested from the environment (e.g. solar, wind, vibration and TE) presents an alternative to batteries, which are bulky and contain a finite amount of energy. Thermoelectric power generation presents many advantages including solid-state operation with no moving parts, long life (∼20 years) and high reliability [5]. The drawbacks of existing thermoelectric generators are low efficiency and large size [5].

The efficiency of TE materials is determined using the figure of merit $ZT = (\alpha^2 T/\rho K_T)$, where α, T, ρ and K_T are the Seebeck coefficient, absolute temperature, electrical resistivity and thermal conductivity, respectively [5]. To maximize the thermoelectric figure of merit (ZT) of a material, large thermopower (absolute value of the Seebeck coefficient), high electrical conductivity and low thermal conductivity are required. Therefore, the performance of these devices depends on the properties of the materials. One of the crucial parameters to be considered in order to improve the thermoelectric properties of the material is their optimum microstructural properties (e.g. grain size, chemical composition and composition homogeneity across a sample). A highly homogenous material will yield improved thermoelectric properties [6, 7]. It has also been previously shown that the grain size has a significant effect on the phonon mean-free path by offering a potentially more favourable carrier scattering mechanism and a much lower lattice thermal conductivity, thus providing the potential for improved thermoelectric devices [8]. Rowe *et al* proposed that scattering at the grain boundaries might be an effective way to improve the efficiency of thermoelectric materials [9].

The best TE materials commercially available today are $Bi_{2-x}Sb_xTe_3$ based, which have a ZT of ∼0.9 at room temperature. However, nanostructured materials have recently attracted great interest because theoretical studies have predicted that efficiency is increased by a factor of ∼3 if the thermoelectric element's 'leg' diameter can be decreased to a size at which quantum confinement and interface scattering effects occur [10].

In order to fabricate thermoelectric devices from $Bi_{2-x}Sb_xTe_3$ nanostructures, various traditional methods, such as laser ablation, solution-based synthesis, vapour-phase growth, thermal evaporation methods and vacuum-based techniques such as metal organic vapour deposition (MOVPD), molecular beam epitaxy (MBE) including liquid phase epitaxy have been used [11–15]. All these methods require either complex parameter optimization or/and are very expensive, and most of them are not compatible with silicon microfabrication processes.

Currently, template-based synthesis has attracted great interest to miniaturize thermoelectric materials using micro/nano-templates from porous alumina, microphotolithography or e-beam lithography [16–19]. Although these techniques offer the unique advantages of a precise size and shape control to fabricate nanowires, these methods have limitations in size, density of thermoelectric elements, complexity and high cost [20, 21].

The current state-of-the-art, presented by Snyder *et al* [18], is a micro-thermoelectric $Bi_{2-x}Sb_xTe_3$ device fabricated by conventional MEMS techniques. This has a limited number of TE elements of 20 μm in length and 60 μm in diameter, and generates a maximum power of ∼1 μW, which is insufficient for most of today's wireless sensor applications.

More recently, the fabrication of Bi and $Bi_{2-x}Sb_xTe_3$ ($x = 1.5$) thermoelectric nanowires has been done by using templates by ion-track irradiation lithography [22, 23]. This technique uses heavy accelerated ions as a source to damage the material, making it susceptible to chemical etching in the direction defined by the irradiation. In the past, this method has been used to evaluate the effect of heavy charged particles on solids, i.e. radiation-induced changes to mechanical, rheological, optical and electrical properties [24, 25]. Different polymers, such as cellulose acetate, dimethyl siloxane, formophenol, polyester, polycarbonate, polyethylene, polyvinyl acetate, were reported in nuclear studies [26]. It has been discovered that ion-track technology can produce low-cost templates for nanowires with a diameter <50 nm and with a high aspect ratio (>1000) [27], and it is a very promising technology for the fabrication of nanostructured devices. Also, it is important to integrate ion-track technology as a part of standard silicon microfabrication batch processes. Hence, only a limited number of polymers can be used and, to date, only polyimide and poly(methyl methacrylate) (PMMA) are compatible with both ion-track technology and MEMS processes.

The pore geometry of etched tracks in polyimide has been extensively investigated [28–31], using the NaOCl etching solution at various pH levels. It was found that the pH value of the etchant plays a crucial role in the selectivity of track etching and the shape of the resulting pores, which depends on both alkalinity and hypochlorite content of the solution. However, there is still an opportunity to decrease the pores' track diameter by using pre-etching chemicals. Vilensky *et al* reported that the use of a strong oxidizer, such as H_2O_2, can significantly increase the etch rate in polyimide and lead to a formation of a smaller pore size [32]. This in turn will lead to a formation of the higher aspect ratio nanostructures.

In the case of PMMA, little research has been done on nanostructured templates by ion-track irradiation. Doobeli *et al* used a very thin layer of 85 nm of PMMA irradiated with MeV C, Ge and I ions that yielded nanopores with diameters between 18 and 45 nm after development [33]. Mistry *et al* [34] and Alves *et al* [35] investigated the effect of the ion-beam lithography on the PMMA thin films using MeV protons for lithography applications. No work has been reported to date on the process development of a suitably thick layer of PMMA in order to reach higher aspect ratio structures.

This paper discusses the development of thermoelectric nanostructures produced by combining the traditional silicon microfabrication techniques with electroplating and submicron ion-track nanolithography for use in a thermoelectric microgenerator, suitable for power harvesting from small temperature gradients. As discussed previously, polyimide and PMMA have been evaluated as the nanostructured templates for $Bi_{2-x}Sb_xTe_3$ (x from 0 to 2)

(a) **Nanotemplate into polymer by iontrack irradiation**

(b) **BiSbTe, p-type thermoelement electroplating**

(c) **Bi₂Te₃, n-type thermoelement electroplating**

(d) **Al junction deposited and patterned**

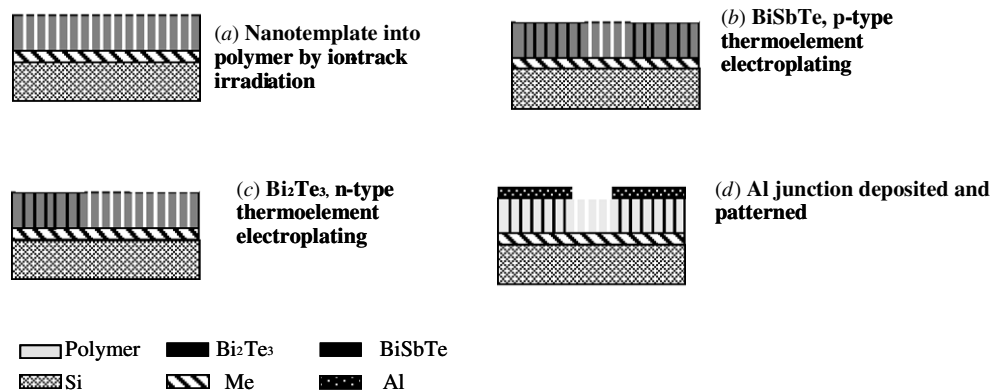☐ Polymer   ▣ Bi₂Te₃   ▤ BiSbTe
▨ Si   ▧ Me   ▦ Al

Figure 1. Process flow.

nanowire electroplating. In addition to their compatibility with silicon microfabrication processes, they can be used on both rigid and flexible substrates, and the pore diameters of the nanotemplates can be controlled to achieve an average diameter size of less than 50 nm. This work presents the electroplating parameters for Bi_2Te_3 nanowires of 80–120 nm into polyimide-nanostructured templates and the development of PMMA-based nanostructured templates. It also reports nanostructures characterization results such as phase analysis, chemical composition and grain size for Bi_2Te_3 nanowires. Preliminary results of the Seebeck coefficient were investigated on thin Bi_2Te_3-electroplated films, and electrical properties of the Bi_2Te_3 bundle nanowires are reported.

2. Experiment

2.1. Microfabrication process

A schematic diagram of the thermoelectric nanostructured generator process flow is shown in figure 1. A thin layer of metal is evaporated onto an oxidized Si wafer, which acts as a seed layer for Bi–Sb–Te electroplating. This is followed by a deposition of a thick layer (20 μm) of polyimide or 10 μm of PMMA. The polymer layers are then exposed to the ion-track irradiation, damaging the material into the parallel track directions. The next step involves wet etching of the irradiated films to open up the nanopores. This stage is followed by photolithography in order to define the areas for n-type Bi_2Te_3 electroplating. Next, n-type Bi_2Te_3 nanowires are electroplated. Then, another photolithography is realized to define the moulds for p-type $Bi_{2-x}Sb_xTe_3$ electroplating and to mask the areas with n-type Bi_2Te_3-electroplated structures. Once p-type $Bi_{2-x}Sb_xTe_3$ nanowire arrays are electroplated, an aluminium layer is evaporated and patterned to form the upper interconnect layers between individual TE elements. The polyimide template is then removed 'freeing' the Bi_2Te_3 and $Bi_{2-x}Sb_xTe_3$ nanoelements. Kapton can be successfully removed by using an N-methylpyrrolidone (NMP)-based solvent without affecting the structural stability of the device. In the case of the PMMA, standard solvents such as acetone or iso-propyl-alcohol (IPA) can be successfully used. Alternatively, a flexible version of the generator may be produced by using the low thermal conductivity Kapton as the main structural support.

## 3. Results

3.1. Polyimide nanotemplate etching

All polyimide samples were irradiated with Pb projectiles of $\sim$2.3 GeV kinetic energy and fluences of 5×10^8 or 5×10^9 ions cm^{-2} at the heavy ion accelerator Unilac at the GSI (Darmstadt). We have studied track etching in polyimide PI2731 wet-type photoresists from HD Microsystems and also dry films of Kapton HN from Dupont of 12.7 μm thickness. Both were spun on/laminated to silicon substrates with and without 200 nm of a gold seed layer for the subsequent electroplating process. Kapton HN foils of 20 μm thickness were also investigated.

Samples irradiated with 5×10^8 ions cm^{-2} and 5×10^9 ions cm^{-2} were pre-etched in an H_2O_2 solution at 60 °C or 90 °C and subsequently etched in a sodium hypochlorite (NaOCl) (13%, pH $\sim$ 12.6) solution at 60 °C. The resulting pores were observed using scanning electron microscopy (SEM) (figures 2 and 3). Depending on the nature of etched polyimide (wet or dry type), etching time, temperature of the solutions (H_2O_2, NaOCl) and pH of NaOCl, the pore diameter varied between 30 nm and 120 nm for different samples of polyimide.

Typically, the smallest pore sizes of 30–50 nm were observed for PI2731, wet-type photosensitive polyimide. However, the adhesion of the wet polyimide onto gold-coated silicon substrates was poor, and further studies on the chemical activation of the gold surface to improve the adhesion between metal and polymer layers are needed.

3.2. PMMA template etching

Two types of PMMA polymers have been used for nanostructured template fabrication: PMMA foil (50 μm thick from Goodfellow) and PMMA wet photoresist (950A11 from Microchem). PMMA layers of 10 μm were spun onto the Au/Cr surface of silicon wafers. All PMMA samples were then irradiated with U$^+$ ions (kinetic energy of
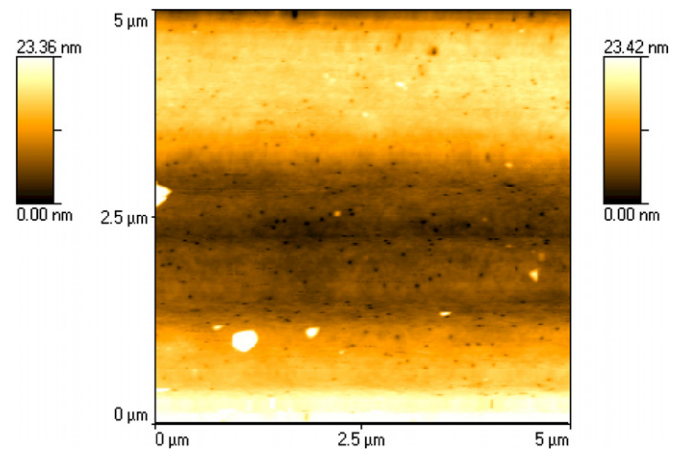
(a)　　　　　　　　　　　　　　　　　　　　　　　(b)
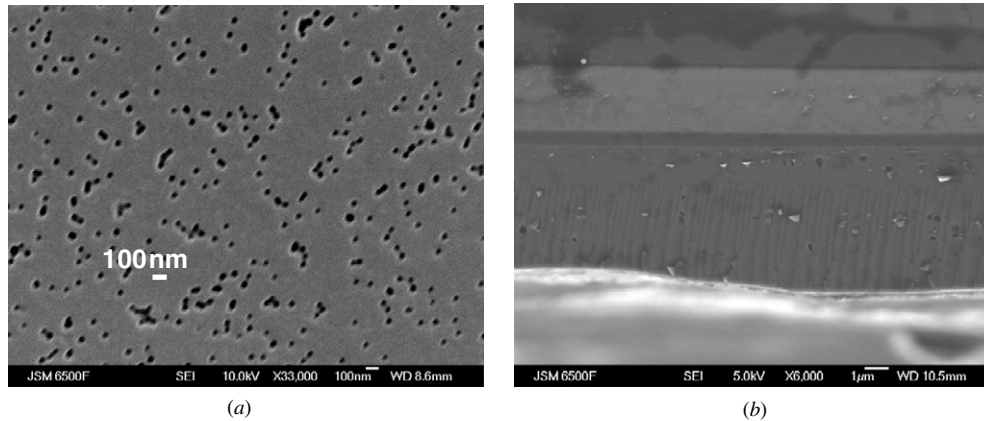
Figure 2. SEM of polyimide, 5×10^9 ions cm^{-2} (PI2731, 10 μm thick), ion-track etched, 40 min in H$_2$O$_2$ (60 °C) followed by 5 min in NaOCl (60 °C). Pore diameters from 30 to 50 nm. (*a*) Top view. (*b*) Cross-section.
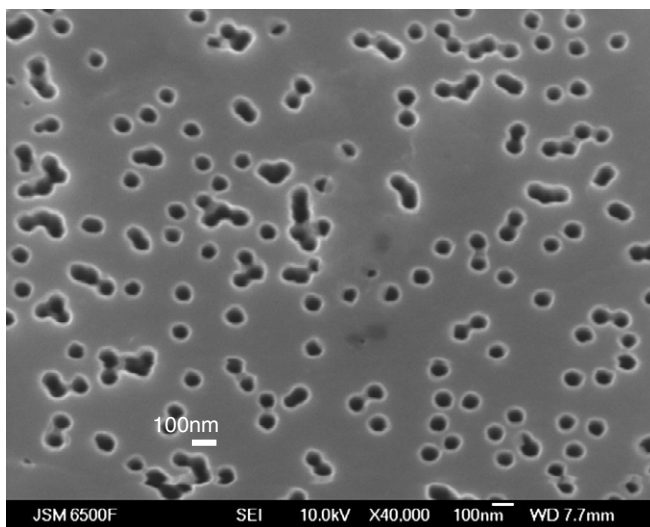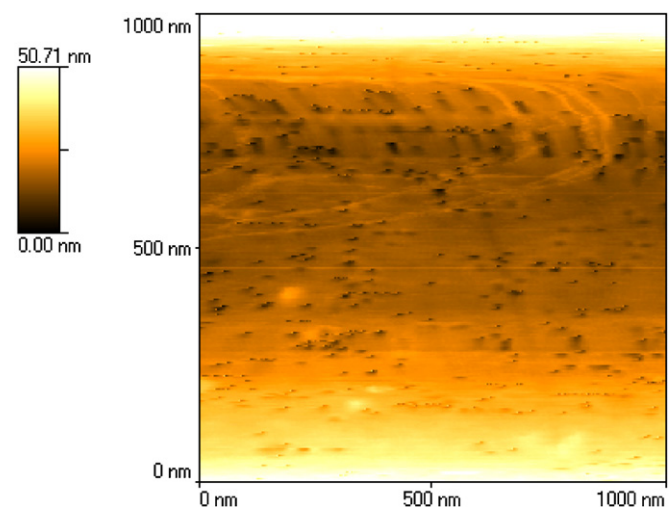

Figure 3. SEM of polyimide (Kapton, 12.7 μm thick), 5×10^9 ions cm^{-2} (Kapton, 12.7 μm thick), ion-track irradiated and etched for 40 min in H$_2$O$_2$ (60 °C) followed by 5 min in NaOCl (60 °C). Pore diameters from 80 to 120 nm.

Figure 4. AFM scan of PMMA 950 10 μm thick, 10^9 ions cm^{-2} ion-track irradiated and etched, 1 h etch in a GG developer. Pore diameters from 30 to 50 nm.

11.4 MeV/nucleon and fluences of 10^8 or 5×10^9 ions cm^{-2}) at the heavy ion accelerator Unilac at the GSI (Darmstadt). Two wet etch solutions were evaluated with the ion-track-irradiated substrates. These were a methyl-iso-butyl-ketone MIBK-based developer (MIBK/IPA) and the 'GG' developer system (a mixture of water and three different organic solvents: 15 vol% water, 60 vol% butoxy-ethoxyethanol, 20 vol% tetrahydro-oxazine and 5 vol% aminoethanol). Both solutions were used at room temperature and constantly mixed on an electromechanical shaker to ensure a uniform wet-etch process. This resulted in the best conditions, a faster development rate and a smoother developed surface. For the PMMA photoresist, these etches resulted in pore diameters of <30 nm (for the MIBK:IPA solution) and ranged from 30 to 50 nm (for the GG solution) (see figures 4 and 5).

This leads to features with an aspect ratio of about 1000:1. For the PMMA foils (50 μm thick), wet-etched pore diameters ranging from 25 to 100 nm were achieved with the GG
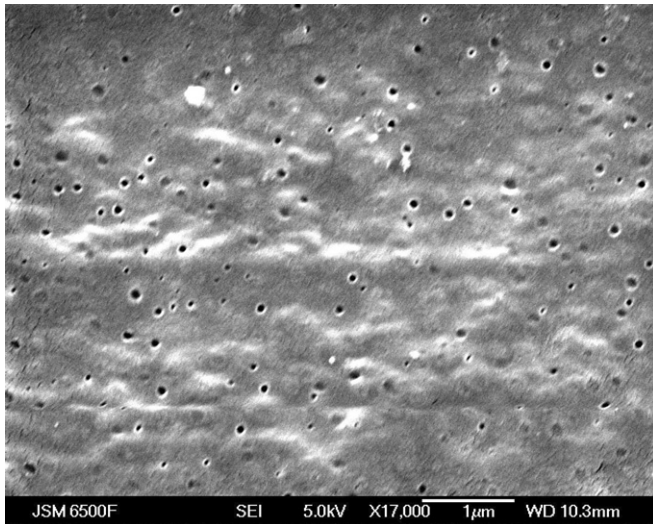

Figure 5. AFM of PMMA 950 10 μm thick, 10^9 ions cm^{-2}, ion-track irradiated and etched, 1 h etch in an MIBK:IPA developer. Pore diameters of <30 nm.

Figure 6. SEM of PMMA foil 50 μm thick, 10^8 ions cm^{-2} ion-track irradiated and etched, 4 h etch in a GG developer. Pore diameters range from 25 to 100 nm.

developer (see figure 6). This study showed that the PMMA 950 photoresist results in higher aspect ratio structures and with good adhesion to the gold-coated silicon substrate.

To image the openings of holes etched along the ion tracks and confirming that the PMMA is sensitive to the development solutions mentioned, the track openings were analysed by atomic force microscopy (AFM) in a non-contact mode. Measurements were carried out with a commercial microscope (Veeco Explorer) operating in air. A high aspect ratio Si nanowhisker cantilever has been utilized to perform a quantitative analysis of the holes which are up to 45 nm in diameter.

3.3. Bi–Te nanowire electroplating

Electroplating of Bi$_2$Te$_3$ nanowires into polyimide templates was carried out by cathodic electrochemical co-deposition of bismuth and tellurium powder dissolved in the aqueous nitric acid using a three-electrode cell with
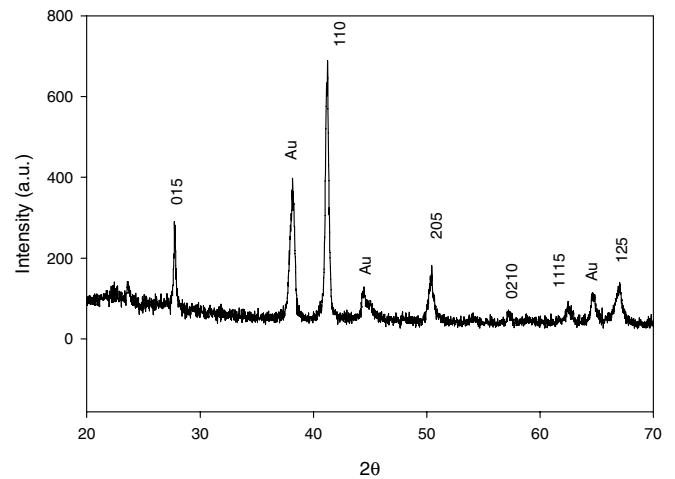

Figure 8. XRD of Bi$_2$Te$_3$ nanowire composition by electroplating.

an Autolab potentiostat/galvanostat. It was found that the electrodeposition conditions (such as current density, deposition potential and temperature) have a significant effect on the Bi$_2$Te$_3$ nanostructure and morphology. The samples were electrodeposited in the plating bath at room temperature. For a range of applied potentials from -0.22 V to 0.03 V versus a saturated calomel electrode (SCE), the resulting Bi$_2$Te$_3$ compounds show a stoichiometric composition. Figure 7 shows Bi$_2$Te$_3$ nanowires electroplated into polyimide nanostructured templates. It can be seen that the average diameter of the nanowires is about 80–120 nm, which is consistent with the pore size of the polyimide template.

3.4. Bi–Te nanowire microstructural characterization

The grain size of the Bi$_2$Te$_3$ nanowires was characterized using a JSM-6500F scanning electron microscope operating at 20 kV. The crystal structures of Bi$_2$Te$_3$ nanowires were investigated using a Siemens D5000 x-ray diffractometer with Cu Kα radiation ($\lambda = 1.5406$ Å). Wide-angle x-ray diffraction spectroscopy (XRD) spectra revealed that the deposited nanowires have a rhombohedral structure, R3 m (figure 8).

(*a*) (*b*)
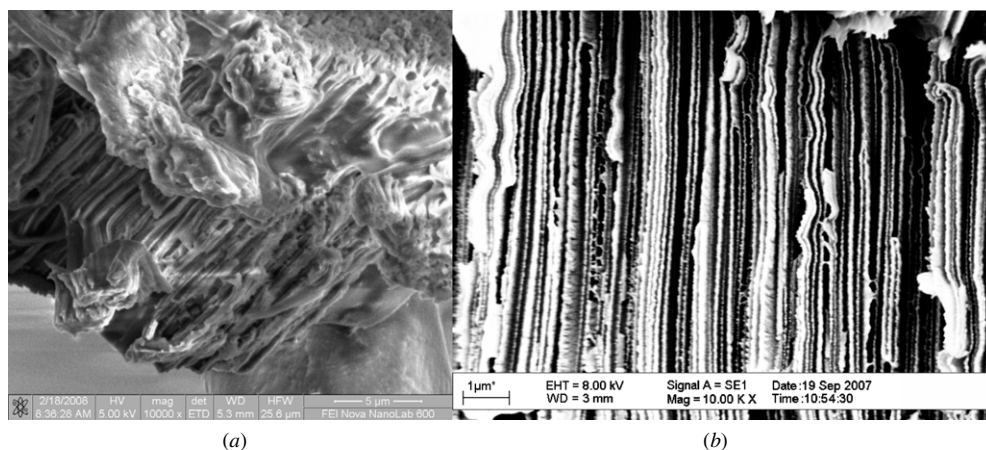
Figure 7. SEM image of a cross section of Bi$_2$Te$_3$ nanowires deposited at -0.2 V versus SCE at room temperature into a polyimide template with a pore diameter of 80 nm to 120 nm. (*a*) 5 μm scale, (*b*) 1 μm scale.
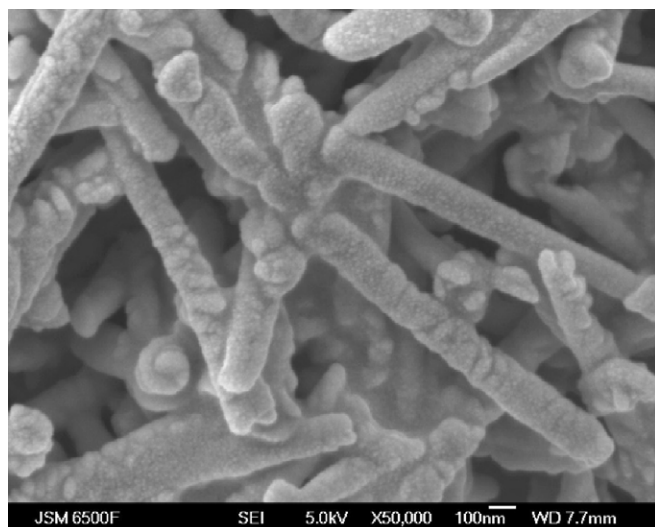
Figure 9. SEM image of Bi_2Te_3 nanowires showing their grain structure.

Table 1. Chemical composition of Bi_2Te_3-electroplated film surfaces by EDS and microprobe analyses.

Theoretical formulation Bi_2Te_3		
Type of analyses	Microprobe	EDS
Bi concentration (at%)	43.37	40.95
Sb concentration (at%)	0.4	0
Te concentration (at%)	56.24	59.05
Analysed composition	$Bi_{2.31}Te_3$	Bi_2Te_3

The standard ICDD PDF card data (82-0358) has been used to identify and index all detected peaks as those belonging to the Bi_2Te_3 crystal with the space group R3 m except for the peaks of Au, which come from the gold seed layer that was used as a working electrode. Therefore, a polycrystalline single-phase Bi_2Te_3 compound was successfully electroplated. According to SEM observations, the electroplated nanowires appeared to have a very fine microstructure with a grain size of the order of tens of nanometres as shown in figure 9.

3.4.1. Chemical composition analyses. The chemical composition of Bi_2Te_3 films and nanowires was determined using energy dispersive spectrometry (EDS) with accuracy measurement of ∼5%, the analysed volume being of the order of μm^3 from the surface. In order to study the homogeneity of the chemical composition across the film surface, microprobe analysis (Cameca, Castaing) on a raw electroplated film surface has been used. The accuracy of the measurements is ∼0.1% and the analysed volume is in the order of 1 μm^3. The chemical composition of Bi_2Te_3 films and nanowires by EDS gave a constant Te content of ∼59.05 at% and a Bi content of 40.95 at%, which is nearly stoichiometric. The chemical composition by microprobe analyses of the binary Bi_2Te_3 showed a Bi excess (table 1). The volume analysed by the microprobe corresponded to a thickness of the order of 1 μm from the film surface.
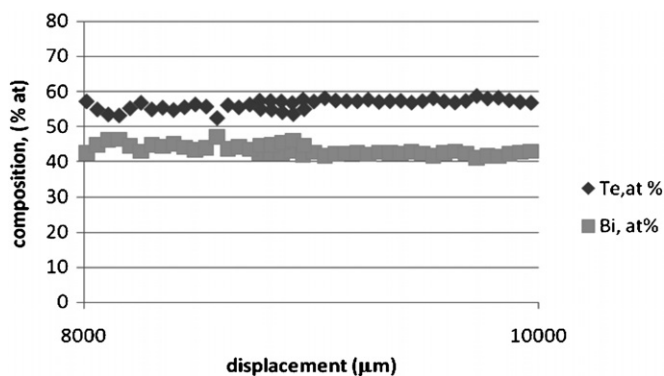
**Figure 10.** Microprobe profiles of Bi_2Te_3-electroplated film surface.

These deviations from the nominal composition match previous observations [12, 36–38]. According to Horak *et al*, this can be explained by native defects (antisite type) in the Bi_2Te_3 structure: in the crystal lattice an excess of Bi atoms takes the place of the Te^{II} sites and thus there is the formation of the defects antisite Bi'_{Te}. Miller and Li showed experimentally that defects of the antisite type predominate in samples with AN excess of Bi [39]. This type of Bi_2Te_3 compound is considered quasi-stoichiometric [12]. The studies by Eyidi *et al* showed that the default structure in Bi_2Te_3 extends up to between 2 and 20 μm in depth [40]. This suggests that a small deviation from the stoichiometric composition can be typically observed in the superficial layer of this material, and varies from one type of thin technology fabrication technique to another. In fact, non-homogeneity of the evolution of the chemical composition through the sample thickness was observed previously [41, 42]. However, this deviation can be solved by the annealing of the native structural defects.

The homogeneity of the chemical composition of Bi_2Te_3 across the electroplated surface was determined from microprobe analysis profiles. Microprobe profiles of Bi (at%) and Te (at%) are reported in figure 10. The variations in the concentration of Bi (at%) and Te (at%) across the samples are in the range of 3%, which is an acceptable value for $Bi_{2-x}Sb_xTe_3$ compounds [43, 44]. Massalsky's phase diagram showed that the homogeneity for the chemical compound Bi_2Te_3 falls into a range of 52–65 at% [44]. These profiles evidenced the chemical composition homogeneity along the surface of the Bi_2Te_3 samples. These chemical composition results show that for binary Bi_2Te_3 alloys, the electroplating technique can be used to reach the stoichiometry and achieve a homogeneous distribution of the elements across the surface. This chemical homogeneity is an important parameter for the performance of thermoelectric materials.

3.5. Thermoelectric properties of Bi_2Te_3-electroplated structures

The Seebeck coefficient α ($\mu V\ K^{-1}$) was determined using a custom-made Seebeck measurement unit, which was calibrated against a reference standard. The measurement accuracy is 5%, using a polycrystalline Bi foil as a reference standard. The system was calibrated using copper-constantan
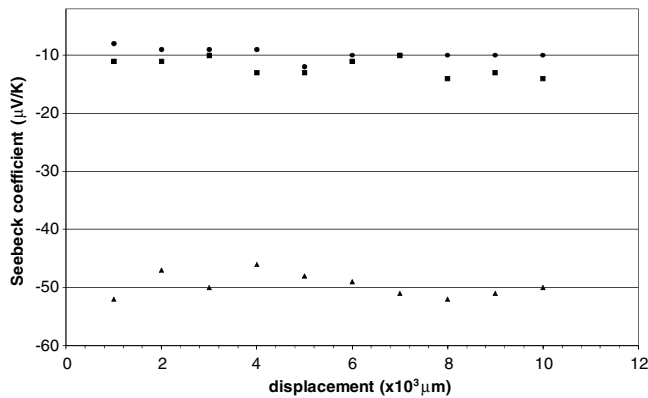
Figure 11. Seebeck coefficient profiles for Bi$_2$Te$_3$-electroplated films.

thermocouples and a high precision Keithley DMM 2000/E digital multimeter with 0.1% accuracy.

The Seebeck coefficient profile was measured along the surface of various raw electroplated Bi$_2$Te$_3$ film samples, and the profiles are reported in figure 11. These profiles evidence the uniformity of the Seebeck coefficient across the surface of the Bi$_2$Te$_3$ samples. The Seebeck coefficient of the Bi$_2$Te$_3$ film had a negative value, which shows n-type of the semiconductor. The maximum value of the Seebeck coefficient for a raw Bi$_2$Te$_3$-electroplated film was -52 μV K^{-1}. Annealing treatments can further improve these values by eliminating various faults in the crystalline structures, which are typical for Bi$_{2-x}$Sb$_x$Te$_3$ compounds.

The *I–V* characteristic of the Bi$_2$Te$_3$ bundle nanowires was measured by a four-terminal method at room temperature (300 K) using the microscope FEI nova nanolab 600 dual beam FIB. The manipulution system was a Zyvex 4 probe system. The tips used for the probes were electropolished tungsten prepared by dc etching, and the measurement system was a Keithley 4200-SCS semiconductor characterization system.

The bundle consisted of Bi$_2$Te$_3$ nanowires with a thickness of 20 μm and a width of 80–120 nm.

The typical *I–V* curve of a Bi$_2$Te$_3$ bundle is shown in figure 12(*a*), which shows linear behaviour confirming good

Ohmic contact with the nanowires. The part of the nonlinearity of the *I–V* characteristics may be due to the potential barrier formed by contacting the sample with a metal wire. From this curve the resistance of the specimen can be estimated to be $\sim$27 GΩ (at I = 0.3 nA), which corresponded to an electric resistivity of $\sim$14 MΩ cm. The high value of the electric resistivity can be due to the mechanical damage of nanowires during the sample preparation for measurements.

4. Discussion

Our investigations on electrochemically deposited wires reveal that the crystallinity and texture can be controlled by the deposition parameters. Bi$_2$Te$_3$ nanowires grown potentiostatically are (1 1 0) textured and agree with the results reported by Chaouni *et al* [45]. SEM associated with energy-dispersive spectrometry, x-ray diffraction, evidenced a microcrystalline structure with a single phase of Bi$_2$Te$_3$ with a preferential crystalline orientation in (1 1 0) plans, which is the preferred texture for maximizing the thermoelectric properties of Bi$_2$Te$_3$ alloys.

The homogeneity of the chemical composition analysis showed that in the case of binary Bi$_2$Te$_3$ alloys, the electroplating technique can achieve a close to stoichiometric chemical composition and an acceptable homogeneous distribution (within 3%) of the elements across the surface. This chemical homogeneity is an important parameter for the performance of thermoelectric materials. In order to achieve a stoichiometric chemical composition, thermal treatment of the samples will be realized to anneal native structural defects of this material; electroplating parameters can also be further optimized. The fine-grained observed microstructure of 6–10 nm is promising for enhanced thermoelectric material properties, by way of reducing the thermal conductivity.

The high electrical resistivity of the Bi$_2$Te$_3$ bundle nanowires can be due to the mechanical damage of the nanostructures while preparing samples for measurements. Thermoelectric properties of Bi$_2$Te$_3$ can be improved by thermal treatment by annealing various defaults of the microcrystalline structure.
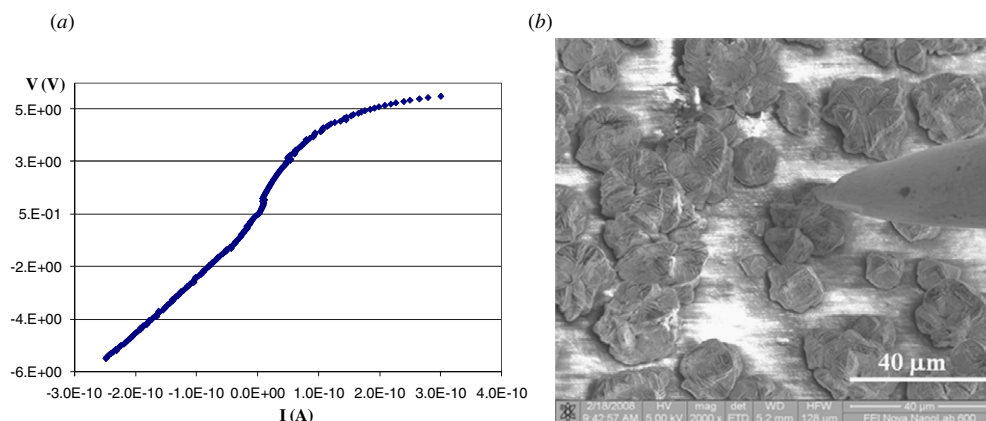
Figure 12. (*a*) *I–V* curve of a Bi$_2$Te$_3$ bundle into polyimide. (*b*) Bi$_2$Te$_3$ bundle nanowires using the Zyvex nanomanipulator.

5. Conclusions

Polyimide (Kapton foil) and PMMA 950 photoresists were found to be promising materials for the realization of a nanostructured thermoelectric generator on flexible and rigid substrates, respectively. These materials are suitable for the fabrication of ion-track nanostructured templates which have been successfully used to form electroplated BiSbTe nanowires, which in turn make up thermoelectric nanostructured generators integrated with silicon microfabrication processes. Polyimide nanotemplates with 30–120 nm pore diameters were fabricated and the PMMA templates yielded <30–100 nm pores. Bi_2Te_3 electroplating of nanowires (80 and 120 nm diameters) was carried out into a polyimide (Kapton 20 μm) ion-track template. Bi_2Te_3 of the R3m structure with close to stoichiometry composition has been deposited with the grain preferential orientation in (1 1 0) and fine grain size (6–10 nm) for optimal thermoelectric properties. An acceptable homogeneity of chemical composition across the surface of the Bi_2Te_3 film (within 3% of variation) was achieved by the low-cost electroplating technique. Optimization of electroplating parameters to decrease the deviation from the stoichiometry, annealing of the structural defects and study of the evolution of the chemical composition through the electrodeposited Bi_2Te_3 film thickness using different microstructural characterization techniques are underway.

Further improvements of the adhesion between the polyimide and Au seed layer are currently being investigated. The etching parameters of an ion-track-irradiated PMMA foil require further optimization to ensure that etching occurs through the entire thickness of the film.

The thermoelectric properties of Bi_2Te_3-electroplated thin films were measured. Future work will include the measurement of the Bi_2Te_3 nanowire microstructural and thermoelectric properties.

Acknowledgments

References

[1] He G, Eckert J, Loser W and Schultz L 2002 Novel Ti-base nanostructure-dendrite composite with enhanced plasticity *Nature Mater.* **2** 33–7

[2] Kuchibhatla S V N T, Karakoti A S, Bera D and Seal S 2007 One dimensional nanostructured materials *Program. Mater. Sci.* **52** 699

[3] Arico A S, Bruce P, Scrosati B, Tarascon J M and Van Schalkwijk W 2005 Nanostructured materials for advanced energy conversion and storage devices *Nature Mater.* **4** 366–77

[4] Law M, Goldberger J and Yang P 2004 *Annu. Rev. Mater. Res.* **34** 83

[5] Rowe D M 1995 *CRC Handbook of Thermoelectrics* (Boca Raton, FL: CRC Press)

[6] Fleurial J P, Borschevsky M A, Ryan M A, Phillips W, Kolawa E, Kacisch T and Ewell R 1997 *Proc. 16th Int. Conf. Thermoelectrics (Dresden, Germany)* pp 641–6

[7] Ivanova L D, Brovikova S A, Zusmann G and Rainshaus P 1994 *Inorg. Mater.* **30** 770–5

[8] Harman T C, Taylor P J, Walsh M P and LaForge B E 2002 *Science* **297** 2229–32

[9] Rowe D M, Shukla V S and Savvides N 1981 *Nature* **290** 5809

[10] Hicks L D and Dresselhaus M S 1993 Use of quantum-well superlattices to obtain a high figure of merit from nonconventional thermoelectric materials *Appl. Phys. Lett.* **63** 3230–3

[11] Watanabe N, Kawamata J and Toshima N 2004 Preparation of protected nanoparticles of bismuth telluride by laser ablation in solution *Chem. Lett.* **33** 1368–9

[12] Goltsman V M, Kudinov V A and Smirnov I A 1972 *Semiconducting Thermoelectric Materials Based on Bi_2Te_3* (Moskow: Nauka)

[13] Mader S 1965 Metastable alloy films *J. Vac. Sci. Technol.* **2** 35–41

[14] Giani A, Pascal-Delannoy F, Boyer A, Foucaran A, Gschwind M and Ancey P 1997 Elaboration of Bi_2Te_3 by metal organic chemical vapor deposition *Thin Solid Films* **303** 1–3

[15] Cho S, Kim Y, DiVenere A, Wong G K, Ketterson J B and Meyer J R 1999 Antisite defects of Bi_2Te_3 thin films *Appl. Phys. Lett.* **75** 1401

[16] Xiaochuan X, Lidong C, Chunfen W, Qin Y and Chude F 2005 Template synthesis of heterostructured polyaniline/Bi_2Te_3 nanowires *J. Sol. State Chem.* **178** 2163–6

[17] Wang W-L, Wan C-C and Wang Y-Y 2006 Investigation of electrodeposition of Bi_2Te_3 nanowires into nanoporous alumina templates with a rotating electrode *J. Phys. Chem.* B **110** 12974–80

[18] Snyder J G, Lim J R, Huang C-K and Fleurial J P 2003 Thermoelectric microdevice fabricated by a MEMS-like electrochemical process *Nature Mater.* **2** 528–31

[19] Chen C L, Chen Y Y, Chen C T, Harutyunyan S R, Lai S J, Chen C D and Lin S J 2008 Thermoelectric properties of Bi_2Te_3 films and nanowire arrays *American Physical Society (APS) 2008 March Meeting (10–14 March)* abstract #H20.009

[20] Fert A and Piraux L 1999 Magnetic nanowires *J. Magn. Magn. Mater.* **200** 338–58

[21] Woo L, Ran J I, Go U, Sele and Nielsch K 2006 Fast fabrication of long-range ordered porous alumina membranes by hard anodization *Nature Mater.* **5** 741–7

[22] Yoo B, Xiao F, Bozhilov K N, Herman J, Ryan M A and Myung N V 2007 Electrodeposition of thermoelectric superlattice nanowires *Adv. Mater.* **19** 296–9

[23] Toimil Molares M E, Chtanko N, Cornelius T W C, Dobrev D, Enculescu1 I, Blick R H and Neumann R 2004 Fabrication and contacting of single Bi nanowires *Nanotechnology* **15** S201–7

[24] Fleischer R L, Price P B and Walker R M 1975 *Nuclear Tracks in Solids* (Berkeley, CA: University of California Press)

[25] Biederman H and Slavinska D 1998 Ion bombardment of organic materials and its potential application *Proc. 1998 Int. Conf. Ion Implantation Technology (Kyoto, Japan)* vol 2 pp 815–9

[26] Fischer B E and Sporh R 1983 Production and use of nuclear tracks: imprinting structure on solids *Rev. Mod. Phys.* **55** 907–48

[27] Lindeberg M and Hjort K 2004 A comprehensive study of ion track enabled high aspect ratio microstructures in flexible circuit boards *Microsyst. Technol.* **10** 608–21

[28] Trautmann C, Brüchle W, Spohr R, Vetter J and Angert N 1996 Pore geometry of etched ion tracks in polyimide *Nucl. Instrum. Methods* B **111** 70–4

[29] Trautmann C, Bouffard S and Spohr R 1996 Etching threshold for ion tracks in polyimide *Nucl. Instrum. Methods* B **116** 429–33

[30] Skupinski M, Toulemonde M, Lindeberg M and Hjort K 2005 Ion tracks developed in polyimide resist on Si wafers as template for nanowires *Nucl. Instrum. Methods Phys. Res.* B **240** 681–9

[31] Klintberg L, Lindeberg M and Thornell G 2001 Sodium hypochlorite as a developer for heavy ion tracks in polyimide *Nucl. Instrum. Methods Phys. Res.* B **184** 536–43

[32] Vilensky A L, Oleinikov V A, Markov N G, Mchedishvili B V and Dontsova E P 1994 Polyimide track membranes for ultrafiltration and microfiltration *Polym. Sci.* **36** 391–9

[33] Doobeli M, Ames F, Musil C R, Scandella L, Suter M and Synal H A 1998 Surface tracks by MeV C60 impacts on mica and PMMA *Nucl. Instrum. Methods Phys. Res.* B **143** 503–12

[34] Mistry P, Gomez-Morilla I, Grime G W, Webb R, Jeynes C, Gwilliam R, Cansell A, Merchant M and Kirkby K J 2005 New developments on the Surrey microbeam applications to lithography *Nucl. Instrum. Methods Phys. Res.* B **231** 428–32

[35] Alves A, Reichart P, Siegele R, Johnston P N and Jamieson D N 2006 Ion beam lithography using single ions *Nucl. Instrum. Methods Phys. Res.* B **249** 730–3

[36] Rowe D M 2006 *Thermoelectrics Handbook Macro to Nano* (Boca Raton, FL: CRC Press)

[37] Stary Z, Horak J, Stordeur M and Stolzer M 1988 Antisite defects in Sb$_{2-x}$Bi$_x$Te$_3$ mixed crystals *J. Phys. Chem. Solids* **49** 29–34

[38] Horak J, Cermak K and Koudelka L 1986 Energy formation of antisite defects in doped Sb$_2$Te$_3$ and Bi$_2$Te$_3$ crystals *J. Phys. Chem. Solids* **47** 805–9

[39] Miller G R and C-Y Li 1965 Evidence for the existence of antistructure defects in bismuth telluride by density measurements *J. Phys. Chem. Solids* **26** 173–7

[40] Eyidi D, Maier D, Eibl O and Westphal M 1998 Defects of Bi$_2$Te$_3$ Peltier device structures *Phys. Status Solidi* a **187** 585–600

[41] Koukharenko E, Frety N, Shepelevich V G and Tedenac J C 2001 Microstructural characterization of ultrarapid quenched bismuth and antimony tellurides alloys *J. Cryst. Growth* **222** 773–8

[42] Naletov V L and Bazhenov D R 1992 *Proc. 3rd Int. Workshop on Thermoelectric Materials* pp 22–3

[43] Mudry S I 1998 The structure of liquid Bi$_2$Te$_3$ alloys near the stoichiometric region *J. Alloys Comp.* **267** 100–4

[44] Massalsky T 1988 *Binary Alloys Phase Diagrams* vol 1 (Metals Park, OH: American Society for Metals)

[45] Chaouni H, Bessières J, Modaressi A and Heizmann J J 2000 Texture prediction of Bi$_2$Te$_3$ electroplated layers using Hartman's theory of crystal growth *J. Appl. Electrochem.* **30** 419–27